Magnetic Resonance Imaging 56 (2019) 161–167

Contents lists available at ScienceDirect

Magnetic Resonance Imaging

journal homepage: www.elsevier.com/locate/mri

Original contribution

A new side-looking downhole magnetic resonance imaging tool

Zhe Sun[a], Lizhi Xiao[a,c,*], Xueli Hou[b], Sihui Luo[a], Guangzhi Liao[a], Yan Zhang[a], Wei Liu[a], Jie Wang[a], Weiliang Chen[a], Zhengduo Wang[a], Lei Li[a], Yifan Wang[a], Feixue Gong[a]

[a] State Key Laboratory of Petroleum Resources and Prospecting, China University of Petroleum, Beijing 102249, China
[b] Technology Center, China Petroleum Logging Co. Ltd., Xi'an 710021, China
[c] Harvard SEAS-CUPB Joint Laboratory on Petroleum Science, 29 Oxford Street, Cambridge, MA 02138, USA

ARTICLE INFO

Keywords:
Side-looking tool
Pre-polarization
Echo time

ABSTRACT

In general, only the depth information can be acquired using the centralized downhole NMR tools. The radial profile information is equally important to the depth. Improving the pad tools, also called side-looking tools, is the appropriate direction for solving this problem. The side-looking downhole measurement can provide depth and radially resolved information of the reservoir. In this research a new side-looking tool which includes main magnets and pre-polarized magnets has been designed and built. The pre-polarized magnets in both sides are used to adjust the homogeneity of magnetic field along the length direction of the instrument and polarize the samples when the tool is moving up and down along the borehole with a speed up to 500 m/h. A winding coil with several frequencies corresponding to different depths has been designed to match the static magnetic field. The sensitive region of this tool is about one-third of a hollow cylinder at every frequency which gives a side-looking image of the borehole wall. We have demonstrated that this new side-looking tool behaves well with an echo time short to 0.25 ms, which ensures the richness and accuracy of the measurements. Such a new side-looking tool is suitable for the detection of unconventional reservoirs.

1. Introduction

Nuclear magnetic resonance (NMR) has been widely used in many fields since it was first discovered in 1945. In oil industry, this technology is mainly used for logging. The early NMR logging tools adopted the geomagnetic field as the B_0 field, and the instrument itself produced only the radio frequency (RF) field as the B_1 field [1]. For many cases, these tools did not behave very well. However, the oil industry did not stop striving to improve the performance of well-logging tools to measure the properties of fluids confined downhole. An alternative way of performing NMR, the "inside-out" concept, was started in 1978 [2]. This unconventional way of implementing NMR, in which stray magnetic and radio frequency fields are used to recover information of arbitrarily large objects placed outside the magnet, could be one of the milestones of the development of modern NMR logging tools.

Since the 1980s, several downhole NMR tools, such as the MRIL-prime [3], CMR [4], MREx [5], MR-Scanner [6], MRIL-XL [7] and so on, have been developed by the oil service companies. Inspired by the "inside-out" concept, all these tools employ magnetic field generated by permanent magnets instead of geomagnetic field. Different arrays of permanent magnets, implemented different functions corresponding to different tools, were developed and combined with suitable RF-coils to excite samples and detect signals. Based on these tools, the information of reservoir evaluation such as porosity, saturation of oil and gas, permeability, pore size, bound water etc. could be obtained.

According to different working modes, these tools can be divided into centralized and decentralized mold. Among the common tools mentioned above, the MRIL-prime is centralized and the others are decentralized, also called pad tools. In general, only the depth information can be acquired using the centralized downhole NMR tools. The radial profile information is equally important to the depth. In many cases, information influenced by strong anisotropy or partial invasion of drilling fluid around borehole will cause problems and may have serious impact to applications. So, it is important to improve the pad tools, also called side-looking tools, to solve these problems.

Each of these tools has its own detecting advantages and features. The side-looking tools designed generate homogeneous or gradient magnetic field. The homogeneous tools, such as CMR, usually has a single working frequency, could obtain the average information of the whole sensitive region. The gradient ones could acquire the depth information and radial profile information simultaneously at multiple frequencies corresponding to different depth slices.

* Corresponding author at: State Key Laboratory of Petroleum Resources and Prospecting, China University of Petroleum, Beijing 102249, China.
E-mail addresses: lizhi_xiao@fas.harvard.edu, xiaolizhi@cup.edu.cn (L. Xiao).

https://doi.org/10.1016/j.mri.2018.09.011
Received 29 July 2018; Received in revised form 11 September 2018; Accepted 13 September 2018

Both these two kinds of downhole NMR tools have their own unique design challenges. In the borehole, the tool is seriously limited by the space size. Thus, compared with the tools on the ground, the magnet assembly of the downhole tool needs a simpler structure that can create a strong enough B_0 field. Magnet structures like MRIL-XL could produce a radial magnetic field. Magnet structures like CMR create a special shape of homogeneous magnetic field. Magnet structures like MREX and MR-Scanner generate circular ring shape of magnetic fields. All these 4 kind magnet structures can be used for decentralized measurement. The first three structures use a combination of multiple magnets. These structures are slightly complicated. And the last two structures adopt soft magnetic material to increase the performance of the antenna. It is also a combination. However, this may lead to new problems because of the complexity of the material and other reasons. Generally, different combinations achieve different functions. For downhole tools, a simpler magnet structure will always be a choice. Thus, the new tool we designed in this research only uses one kind of magnets as the main magnet structure and did not adopt soft magnetic material.

2. Design and theory

This tool is designed to work in decentralized mode and could be used in both large borehole and slim borehole. Considering this, the diameter of this tool is limited to 5 in. Within this range, magnets, RF antennas and their frameworks are necessary to be included. In addition, a push device is required to keep the tool contact with the wall of the borehole. The area where B_0 and B_1 are orthogonal and satisfied the relationship of Larmor frequency is the sensitive volume. Different sensitive volumes correspond to different operating frequencies constitute the detection area. The working mode of this new tool is shown in Fig.1(a). The red and blue arrows illustrate the vector of B_0 and B_1 respectively. The blue circle is the isocline of B_0 strength. The rainbow color lines are the isoclines of B_1 strength that correspond to different sensitive volume slice. The internal structure of this new tool is shown in Fig. 1(b).

The prototype magnet structure of this new tool is designed in a two-dimensional plane based on the characteristics of the wireline logging tools. As a result, it is designed as a single bar, consists of multiple same magnetic blocks, with a length of about 2.25 m. This prototype behaved well for static measurement. However, when the tool is moving up and down along the borehole, the signal to noise ratio reduced greatly. That may be caused by some long relaxation components which are not be well polarized. To solve this problem, we improved it with three structure groups which include a group of main magnets in the middle and two groups of additional magnets in both sides. The total length of the new tool is about 1.96 m. The middle part is the main magnet structure which is the same shape as the prototype but with a much shorter length of about 1.2 m. The pre-polarized magnets are located at both ends of the magnet assembly [8]. The two pre-polarized magnets are the same and the length of them is 0.3 m. Either of them consists of two kinds of magnet blocks and a piece of iron. Magnet A and B have the same magnetic properties but stronger than the main magnets. The detailed structure of the new magnet assembly is shown in Fig. 2.

The main magnet structure corresponding to the measured area, similar to the prototype but with a much shorter length, produce the target B_0 field. The additional magnets, also named the pre-polarized magnets, in both sides are adopted to adjust the homogeneity of magnetic field and pre-polarize the samples. Among them, the field strength of each additional magnet is much stronger than the target field strength. The role of this part is designed as quickly polarizing the samples.

There will be relative motion between the tool and samples when logging. It can be considered as the samples move though the detection area of the tool with the logging speed. The magnetization of samples is influenced by both the strength of magnetic field and the polarization time. The logging speed and the magnet length determine the polarization time. The faster the speed is the longer the magnet length needed. When the samples move out the pre-polarized part with a suitable speed the magnetization is higher than the target magnetization. The field strength of the gap between the pre-polarized magnets and the main magnets is much lower than the field strength of pre-polarized part, where the magnetization can be rapidly “pulled down”. Thus, when the sample arrives at the measured area, the magnetization can get close to the target magnetization.

After the samples move over the pre-polarized magnets and the gap, the magnetization is expressed as Eq. (1):

$$M = M_A(1 - e^{-t/T_1})e^{-\frac{t-t_A}{T_1}} + M_B\left(1 - e^{-\frac{t-t_A}{T_1}}\right) \quad (1)$$

where M is the magnetization of the samples moving into the measuring area, M_A is the magnetization when samples in pre-polarized magnets get into equilibration, M_B is the magnetization when samples in gap between pre-polarized magnet and main magnets get into equilibration, t is the time for the samples move through the pre-polarized magnets and the gap, t_A is the time for the samples move through the pre-polarized magnets. It worth noting that the equilibrium magnetizations of samples are different in the magnetic field with different strength. In Eq. (1), M_A and M_B correspond the average B_0 strength of the pre-polarized magnets and the gap.

Generally, T_1 value of most samples is between 0 and 10 s. Thus, the new tool should ensure that those samples can reach the target magnetization after the samples move through the pre-polarized magnets.

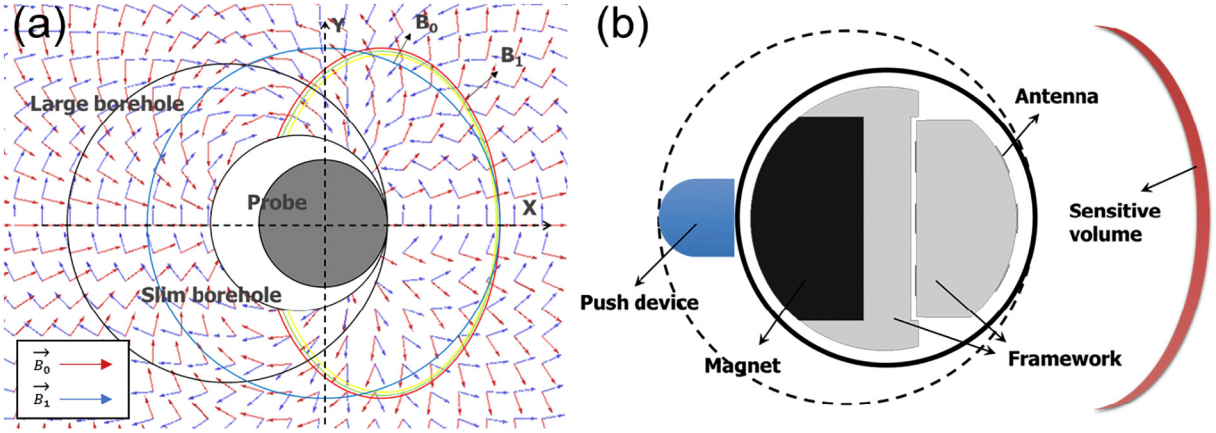

Fig. 1. The working mode and internal structure of the new side-looking tool. (a) is the working mode. (b) is the internal structure.

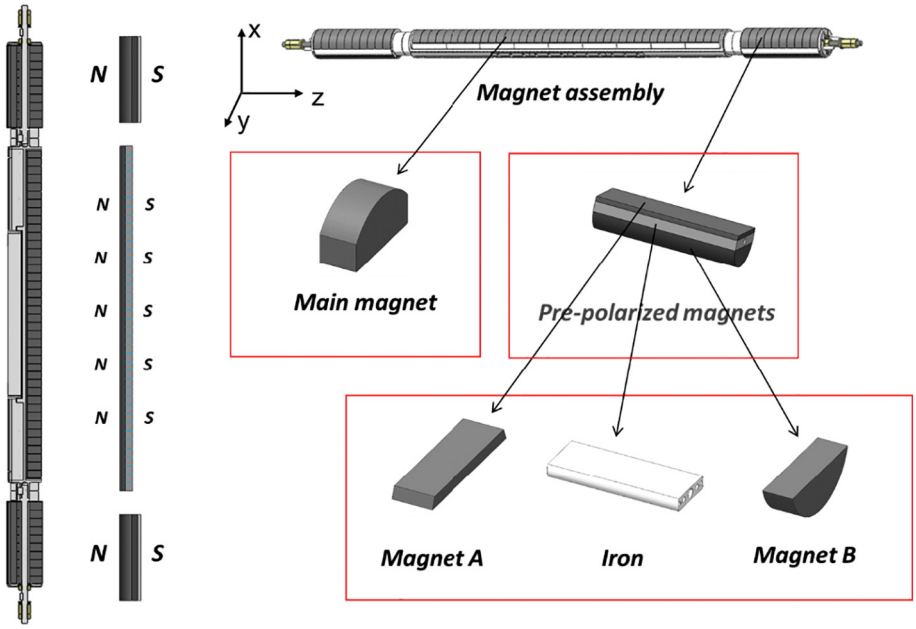

Fig. 2. The detailed structure of the new magnet assembly.

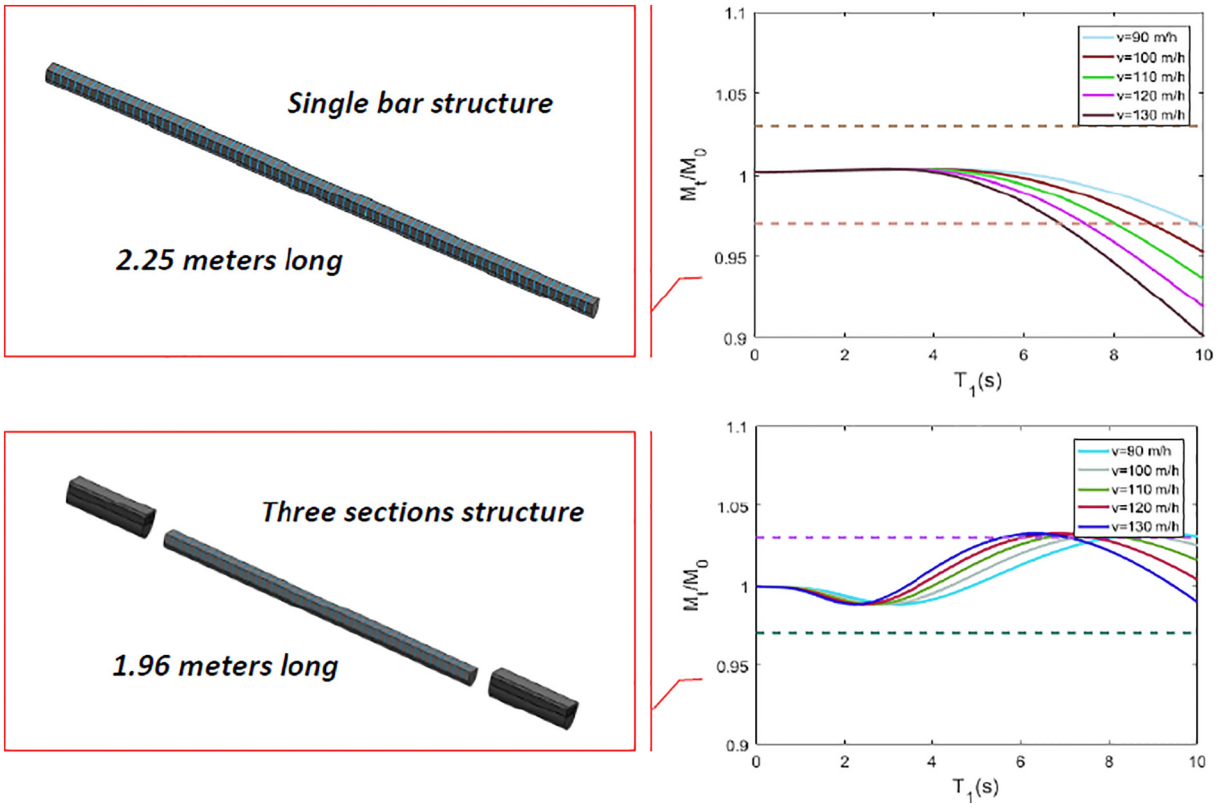

Fig. 3. The polarization efficiency of both prototype and the new magnet assembly.

By performing continuous simulation, the optimized polarization efficiency of both the prototype tool and the new tool is obtained by Eq. (1) and shown in Fig. 3. It can be seen that the polarization efficiency of the new tool can reach 95–105% of the target magnetization after the samples moves over the pre-polarized magnets with a logging speed of 130 m/h. Moreover, even with 50% of the target magnetization the new tool could obtain the signal effectively. As a result the logging speed of the new tool is up to 500 m/h. Compared to the prototype, the new tool can polarize longer relaxation components of the sample in a shorter time.

The corresponding antenna is consisted of coil and framework. The coil is made up of copper stripe wounded around the framework that is made of peek material of 3-turns. The whole antenna is fixed at the center of the other side of the tool. When an excitation current is applied to the antenna, it will produce flux line of B_1 field as shown in Fig. 4. The total length of the antenna is 0.6 m due to the tolerance of 10% inhomogeneity along with z-axis in the sensitive region.

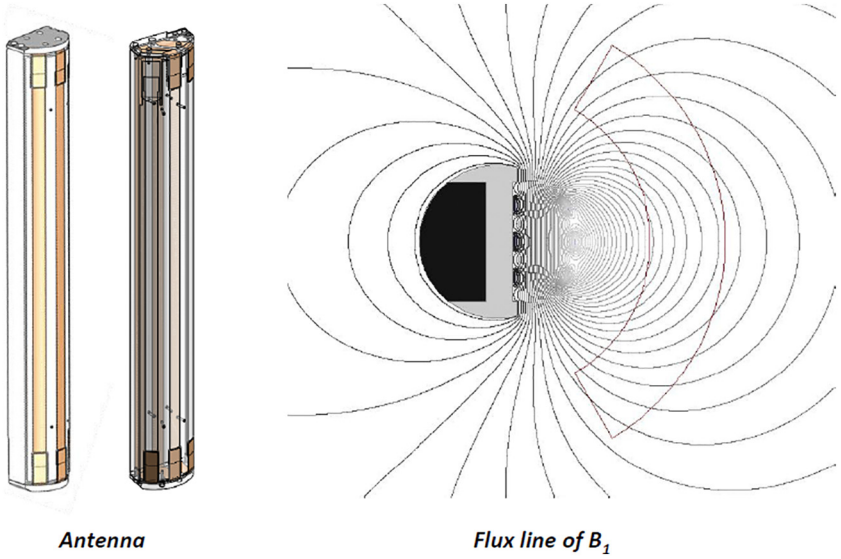

Fig. 4. The structure of the antenna and the corresponding B_1 flux line.

3. Simulation

To some extent, the distribution of B_0 determines the detection area shape of the tool. Fig. 5 shows the simulation result of B_0. The distribution of B_0 on the cross-section is shown in Fig. 5(a). Meanwhile, its vector is shown in Fig. 5(b). With these two results, the B_0 distributions away from the tool on x-axis direction and along z-axis at different detection depths could be obtained. The relationship between the intensities of B_0 and the detection depths is shown in Fig. 5(c). Due to the design objective, the operating frequencies should be between 500 kHz and 950 kHz. As a result, the detection depths should be within this range. Fig. 5(d) is the distribution of B_0 along with z-axis at these 2 boundaries of detection depth.

Considering the eddy current effects, the antenna could not be simulated alone. The framework and the magnet should be import to the simulation either as shown in Fig. 6 (a). The distribution of B_1 is shown in Fig. 6 (b). By changing the distance between the wires, different shapes of B_1 distributions could be obtained. A B_1 field that has the most similar outline with B_0 field is the best choice.

After simulation of B_0 and B_1, a sensitivity map to ensure whether

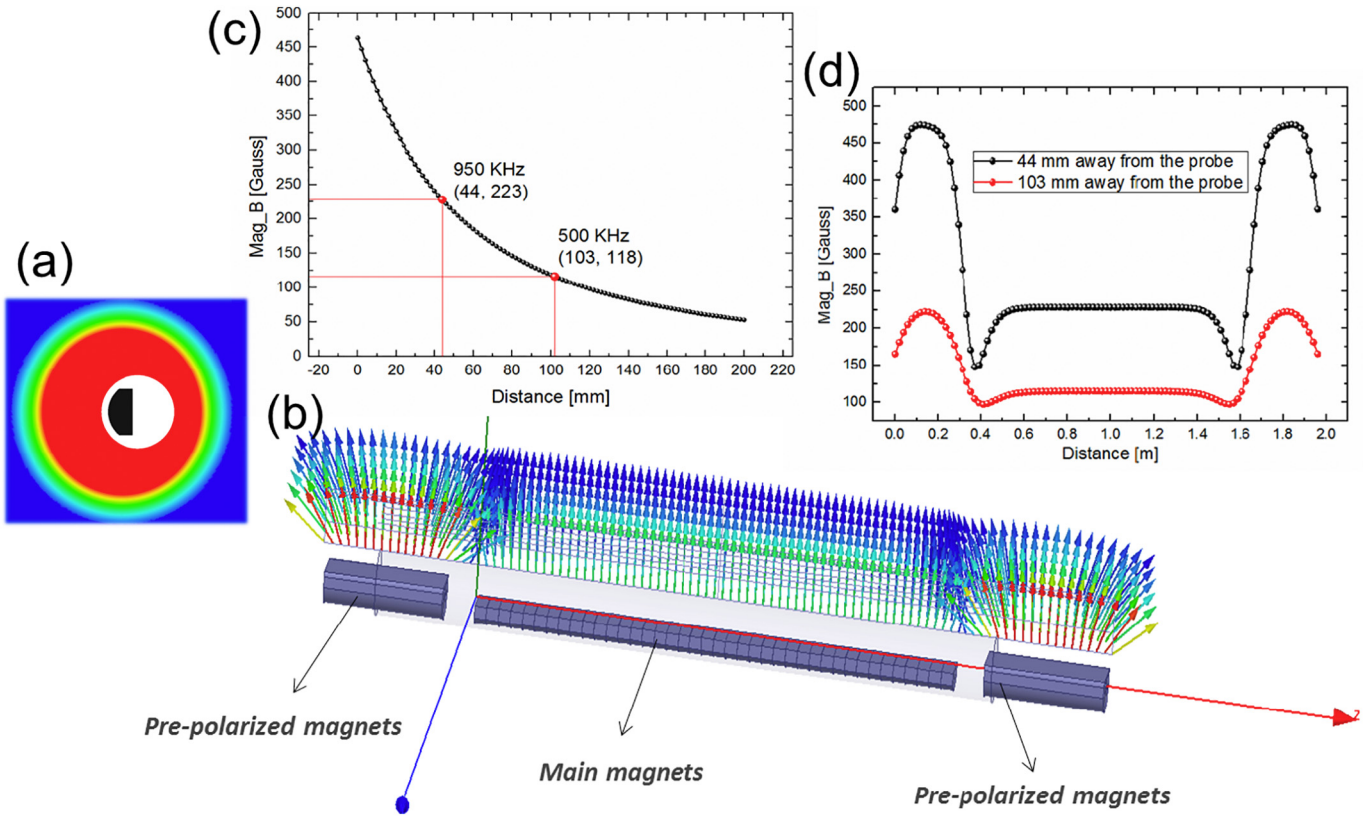

Fig. 5. The simulation result of B_0. (a) is the distribution of B_0 on the cross section parallel to x-y plane. (b) is the vector of B_0 on x-z plane. (c) is the relationship between the intensity of B_0 and the detection depth. (d) is the distribution of B_0 along with z-axis at the 2 boundaries of detection depth.

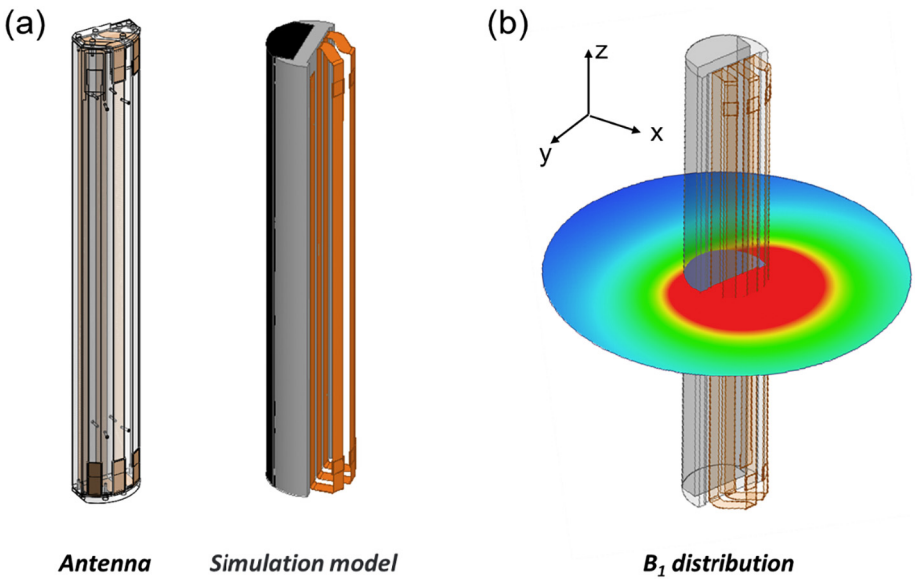

Fig. 6. Simulation of B_1 field. (a) is the antenna and its simulation model. (b) is the distribution of B_1.

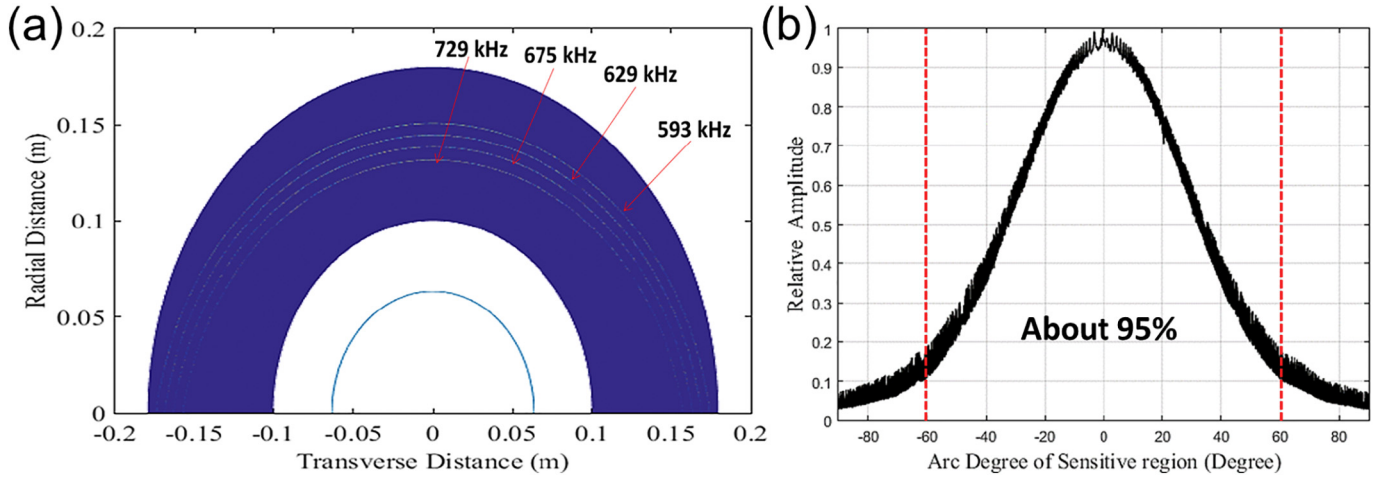

Fig. 7. The sensitivity map of the tool. (a) is the sensitivity map of 4 different operating frequencies. (b) illustrates the contribution of the signal intensity in different arc degree.

Table 1
The measured parameters of the antenna at different operating frequencies.

Resistance (ohm)	Inductance (μH)	Frequency (kHz)	Q value
0.112	2.51	500	70.4
0.117	2.51	600	80.9
0.124	2.51	700	89.0
0.129	2.51	800	97.8
0.129	2.51	900	110.0
0.133	2.51	1000	118.6

the design satisfy the purpose or not is presented. In this simulation, T_E = 1.2 ms, Pulse length = 70 μs. Fig. 7(a) shows the sensitivity map of 4 different operating frequencies [9].The bright dots illustrate the signal. The brighter the dots are the higher intensity the signal is. Moreover, Fig. 7(b) reflects the arc degree of sensitive region. Nearly 95% of the total signal intensity is contributed by the region within 120°. As a result, the shape of the sensitive volume is tile-shaped of about 120° width.

4. Implementation & Experiment

After simulation, this tool has been implemented and measured. The magnet assembly has been characterized by a three-dimensional magnetic field measurement. The measured B_0 field matches well with the simulation result. The antenna has been measured either, and the results are shown in Table 1.

After the implementation, some basic experiments in water tank (fulfilled with doped water) have been taken to verifying whether the tool work. Fig. 8 shows the multi-frequency measurement. The electronic adopted, shown in Fig. 8(a), is the MRT SYSTEM (CPL. Co. Ltd) with the experiment parameters: T_E = 1.2 ms, Pulse length = 70 us, V_{PP} = 2000 V. The horizontal and vertical axes are the number of echo and the relative amplitude correspondingly in Fig. 8(b).The main reason that the amplitudes of these echo trains are different is that the 90° pulse adopted in this experiment is calibrated at the frequency of 728.8 kHz. Meanwhile, the lower frequency corresponds the deeper detection depth.

The further experiments of different T_E and T_W at every single frequency, for example 629.4 kHz, have been taken after the multi-frequency experiment. Fig. 9(a) shows the echo trains for different waiting

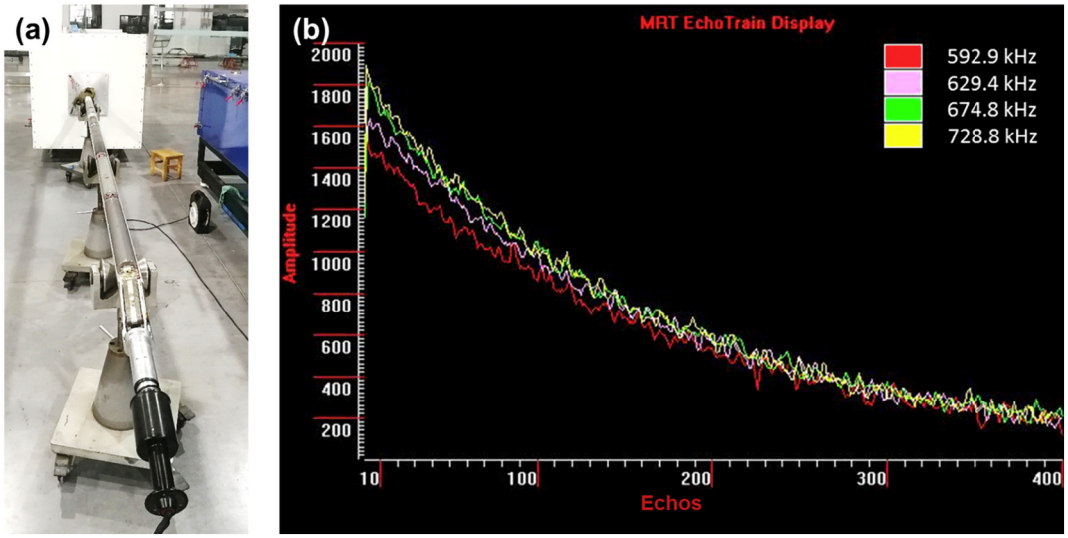

Fig. 8. Multi-frequency measurement. (a) shows the experiment in the water tank. (b) is the echo trains.

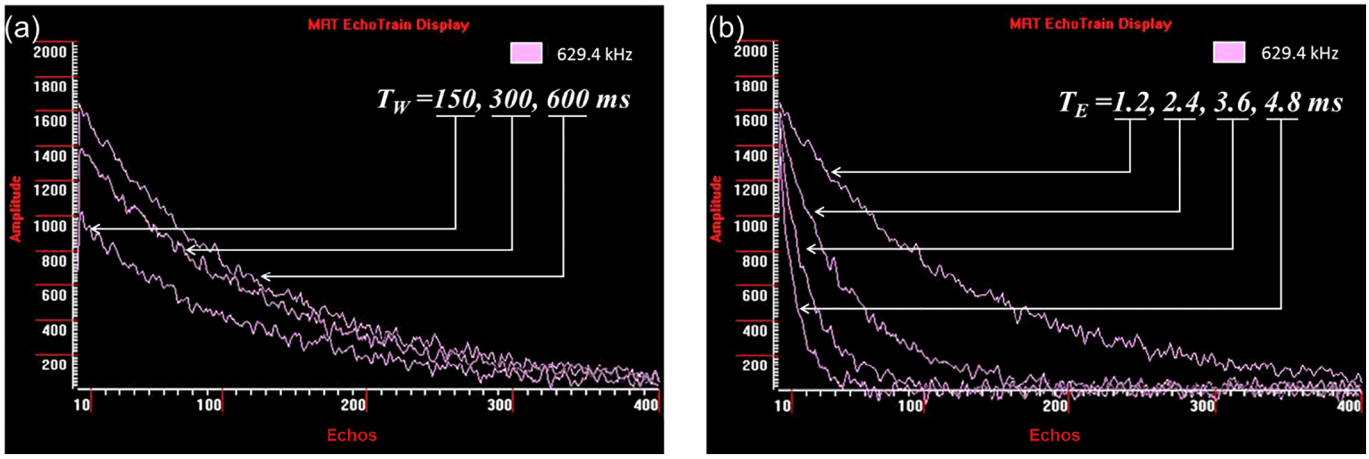

Fig. 9. Experiment of different T_E and T_W at a single working frequency (629.4 kHz as an example).

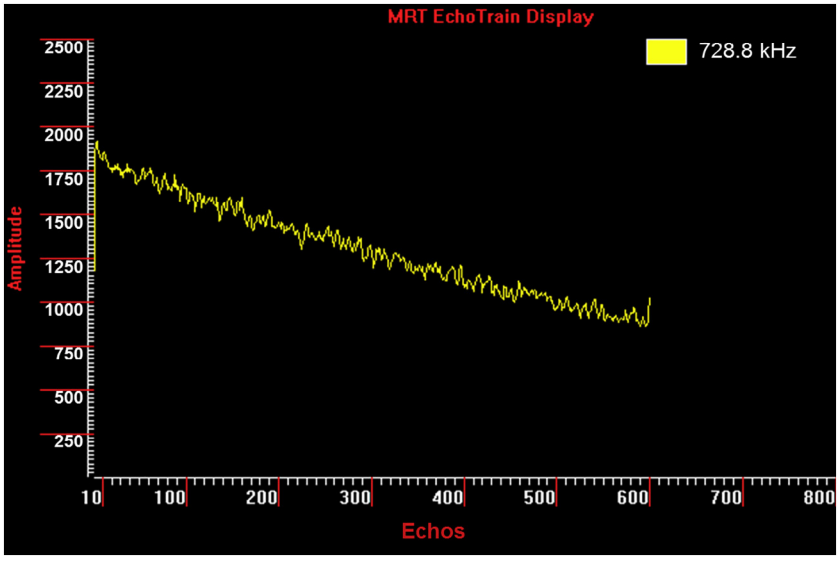

Fig. 10. Experiment of T_E = 0.25 ms at 728.8 kHz.

time at 629.4 kHz. The echo amplitudes change obviously with different waiting time of 150, 300 and 600 ms. The longer the waiting time is the higher the signal amplitude is. Fig. 9(b) is the echo trains for different echo time at the same working frequency. The echo decay rates change significantly with different echo time of 1.2, 2.4, 3.6 and 4.8 ms. It is worth noting that the horizontal axis in Fig. 9 is the number of echoes. The decay time is the product of the echo time and the number of echoes. The decay time of the curves should be the same when measuring the same sample. This means the longer the echo time is the faster the curve decays in the same number of echoes as shown in Fig. 9(b).

In many cases, the shortest echo time of a side-looking tool determines the richness and accuracy of the data it can collect at downhole. Therefore, another experiment for searching the shortest T_E has been taken with the experiment parameters of: T_w = 800 ms, Pulse length = 50 us, V_{PP} = 2600 V. The initial T_E is 0.6 ms and then decreases in steps of 0.05 ms. The final result is 0.25 ms and is shown in Fig. 10. This result is limited by the protection program of the electronic. The electronic we adapted does not work with a T_E less than 0.25 ms.

5. Conclusions

A new side-looking downhole MRI tool has been developed, which can effectively obtain depth and radial profile information. The pre-polarized magnets on both sides make the magnetic field distribute more homogeneous along with z-axis and could polarize the samples effectively at a speed up to 500 m/h. According to the sensitivity map, the sensitive volume of this tool is about one-third of a hollow cylinder at every frequency, which would provide a side-looking information of the borehole wall. The shortest T_E of the new tool is no more than 0.25 ms which ensures the richness and accuracy of the measurements.

There are still lots of things to do in the future, including optimization of probe, electronics and the software. More experiments and the results will be presented in later works.

Acknowledgement

This work was supported by National Natural Science Foundation of China (Grant No. 21427812), National major research and development project (2017ZX05019-002-008 and 2016ZX05021-001-005), CNPC major research and development project (ZYCJJZJS2017006).

References

[1] Brown RJS. Nuclear magnetism logging. Pet Trans AWME 1960;219(8):199–207.
[2] Cooper RK, Jackson JA. J Magn Reson 1980;41(3):400–5.
[3] Coates GR, Xiao LZ, Prammer M. NMR logging principles and applications. USA: Gulf Professional Publishing; 1999.
[4] Kleinberg RL, Sezginer A, Griffin DD, et al. Novel NMR apparatus for investigating an external sample. J Magn Reson 1992;97(3):466–85.
[5] Reiderman A, Beard DR. Side-looking NMR probe for oil well logging. US, US 6580273 B2. 2003.
[6] Toufaily AK, Sezginer A, Jorion B, Depavia LE. Downhole NMR tool having a programmable pulse sequencer. US, US 6400147 B1. 2002.
[7] Prammer MG, Menger S, Knizhnik S, et al. Systems and methods for deep-looking NMR logging. US. 7733086. 2010.
[8] An Improved NMR Tool Design For Faster Logging, Cao Mirth C, et al. SPWLA-1999-CC. Society of petro-physicists and well-log analysts source SPWLA 40th annual logging symposium, 30 May–3 June. Oslo: Norway Publication Date; 1999.
[9] Hürlimann MD, Griffin DD. Spin dynamics of Carr–Purcell–Meiboom–Gill-like sequences in grossly inhomogeneous b0, and b1, fields and application to NMR well logging. J Magn Reson 2000;143(1):120–35.